Supporting information

Facile Synthesis of Iron Doped Rutile TiO_2 Photocatalyst for Enhanced Visible-light-driven Water Oxidation

Junqing Yan,[a,c] Yunxia Zhang,[c] Shengzhong Liu,*[c] Guangjun Wu,[a,c] Landong Li*[a,b] and Naijia Guan,[a,b]

[a] *School of Material Science and Engineering & National Institute for Advanced Materials, Nankai University, Tianjin, 30071, P.R. China*

[b] *Key Laboratory of Advanced Energy Materials Chemistry (Ministry of Education), Collaborative Innovation Center of Chemical Science and Engineering, Tianjin, 30071, P.R. China*

[c] *Key Laboratory of Applied Surface and Colloid Chemistry (Ministry of Education); Institute for Advanced Energy Materials, School of Materials Science and Engineering, Shaanxi Normal University, Xi'an, 710119, P. R. China*

* To whom correspondence should be addressed

E-mail: szliu@dicp.ac.cn (S. Liu) & lild@nankai.edu.cn (L. Li)

Experiments and Methods

Sample preparation

All of the chemical reagents of analytical grade were purchased from Alfa Aesar Chemical Co. and used as received without further purification.

In a typical synthesis of Fe-TiO_2, 10 mL titanium tetrachloride ($TiCl_4$) was dropwise added into 30 mL ice water under stirring to prepare a transparent $TiCl_4$ aqueous solution. Then, a certain amount of ferric chloride ($FeCl_3$) was added into the above solution. After further stirring for 30 min, the mixture was rapidly heated to 373 K to remove water and hydrogen chloride. The obtained light yellow powder was then calcinated in a muffle furnace at 773K in flowing air for 4h. The as-synthesized samples were further treated by 0.01M hydrochloric acid aqueous solution reflux at 343K for 4h to remove the surface iron oxides. The final iron content was analyzed through ICP-AES. The reference rutile TiO_2 was synthesized through a similar process but no $FeCl_3$ was added.

Characterization Techniques

The X-ray diffraction (XRD) patterns of studied samples were recorded on a Bruker D8 ADVANCE powder diffractometer using Cu-K radiation (λ = 0.1542 nm) at a scanning rate of 4^o/min in the region of $2\theta = 20\text{-}80^o$.

Raman analysis was carried out on a Renishaw InVia Raman spectrometer and the spectra were obtained with the green line of an Ar-ion laser (514.53 nm) in micro-Raman configuration.

Diffuse reflectance ultraviolet-visible (UV-Vis) spectra of studied samples (*ca.* 20

mg diluted in ca. 80 mg $BaSO_4$) were recorded in the air against $BaSO_4$ in the region of 200-800 nm on a Varian Cary 300 UV-Vis spectrophotometer.

Transmission electron microscopy (TEM) images were taken on a FEI Tecnai G^2 F20 electron microscope at an acceleration voltage of 200 kV. A few drops of alcohol suspension containing the sample were placed on a carbon-coated copper grid, followed by evaporation at ambient temperature.

X-ray photoelectron spectra (XPS) were recorded on a Kratos Axis Ultra DLD spectrometer with a monochromated Al-Ka X-ray source (hv=1486.6 eV), hybrid (magnetic/electrostatic) optics and a multi-channel plate and delay line detector (DLD). All spectra were recorded by using an aperture slot of 300*700 microns, survey spectra were recorded with a pass energy of 160 eV and high-resolution spectra with a pass energy of 40 eV. Accurate binding energies (±0.1 eV) were determined with respect to the position of the adventitious C 1s peak at 284.8 eV. Valence band XPS (VB XPS) of samples were measured on PHI Quantera XPS Scanning Microprobe spectrometer using Al-Kα X-ray source (hv=1486.6 eV). The energy scales are aligned by using the Fermi level of the XPS instrument (4.10 eV versus absolute vacuum value).

Mott-Schottky plots were obtained using a three-electrode cell electrochemical workstation (IVIUM CompactStat). The saturated Ag/AgCl and platinum foil (2×2 cm^2) were used as the reference electrode and the counter electrode, respectively. The sample of 1 mg was dispersed in 1 mL anhydrous ethanol and then evenly grinded to slurry. The slurry was spread onto ITO glass and the exposed area was kept at 0.25

cm^2. The prepared ITO/samples was dried overnight under ambient conditions and then used as the working electrode. The measurements were carried out at a fixed frequency of 1 kHz in 0.5 M Na_2SO_4 solution in the dark.

Scanning electron microscopy (SEM) images of samples were taken on a field emission scanning electron microscope (FE-SEM, Hitachi S-4800).

Photocatalytic evaluation

Photocatalytic oxygen evolution was performed in a top-irradiation-type Pyrex reaction cell connected to a closed gas circulation and evacuation system under the irradiation of Xe lamp with different optical reflector and/or filter. In a typical experiment, catalyst sample of 100 mg was suspended in *ca.* 100 mL 0.01 M $AgNO_3$ aqueous solution in the reaction cell. After evacuated for 30 min, the reactor cell was irradiated at a constant temperature of 298 K under stirring. The gaseous products were analyzed by an on-line gas chromatograph (Varian CP-3800) with a thermal conductivity detector.

The apparent quantum yield was measured using the same experimental setup for the photocatalytic oxygen evolution, but with additional band pass filters to obtain monochromatic light λ=350, 405, 420, 475, 550 nm and 700nm). The power density was measured to be *ca.* 1.8 (λ=405 nm), 1.5 (λ=420 nm) or 1.6 mW/cm^2 (λ=475 nm) using a calibrated photodiode and the quantum yield was calculated by the following equation:

$$QY = \frac{number\ of\ reacted\ electrons}{number\ of\ incident\ photons} * 100\% = \frac{number\ of\ evolved\ O_2\ molecules * 4}{number\ of\ incident\ photons} * 100\%$$

Photocatalytic Rhodamine B (RhB) degradation was performed in a top-irradiation-

type Pyrex reaction cell. In a typical experiment, catalyst sample of 50 mg was suspended in *ca.* 100 mL of 8 mg/L the RhB and stirred for 5 h to establish an adsorption and desorption equilibrium. Then, the reactor cell was irradiated at a constant temperature of 298 K under stirring with oxygen bubbled in. The supernatant was analyzed on a Hitachi U-3900/3900H spectrophotometer.

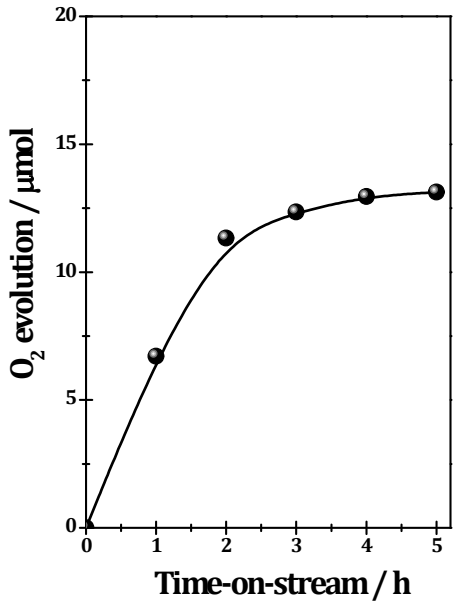

Figure S1 Visible-light-driven water oxidation to oxygen over sub-10 nm rutile TiO_2

Reaction conditions: 0.1g photocatalyst, 100 mL 0.01M $AgNO_3$ aqueous solution

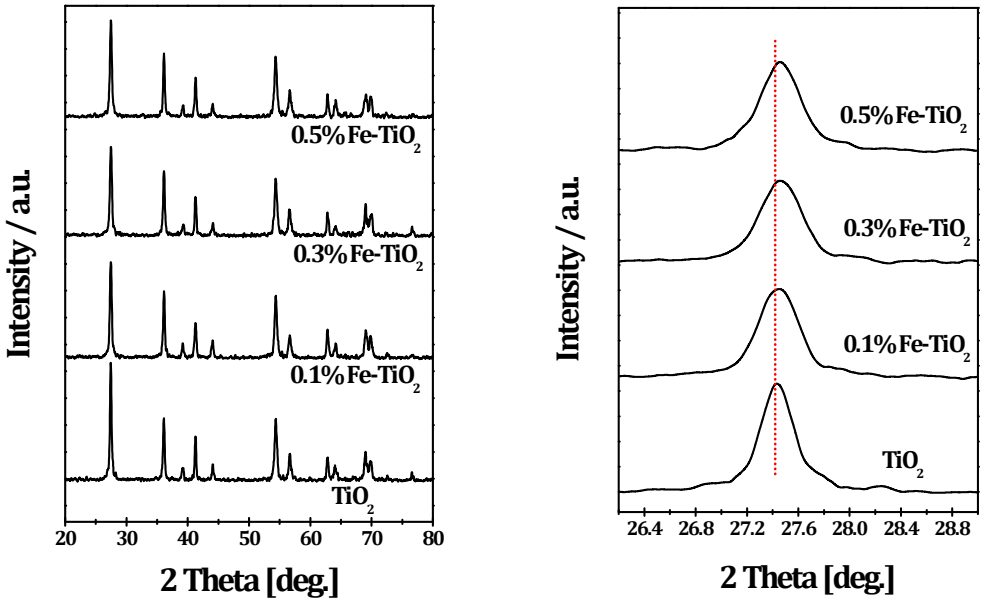

Figure S2 XRD patterns of rutile TiO_2 and Fe doped rutile TiO_2 under study and the magnified view of (110) reflection

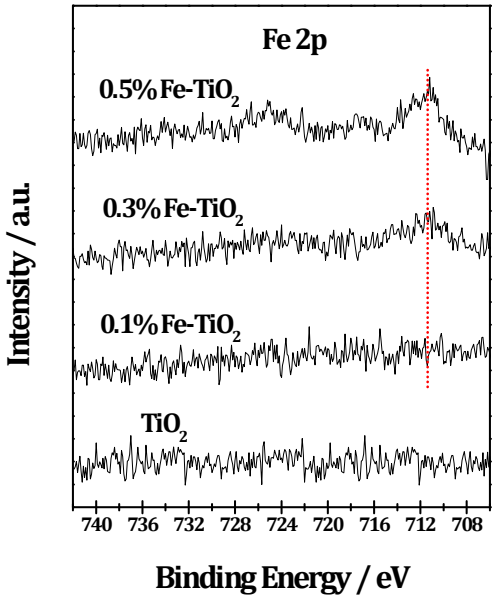

Figure S3 Fe 2p core-level XP spectra of rutile TiO_2 and Fe doped rutile TiO_2 samples

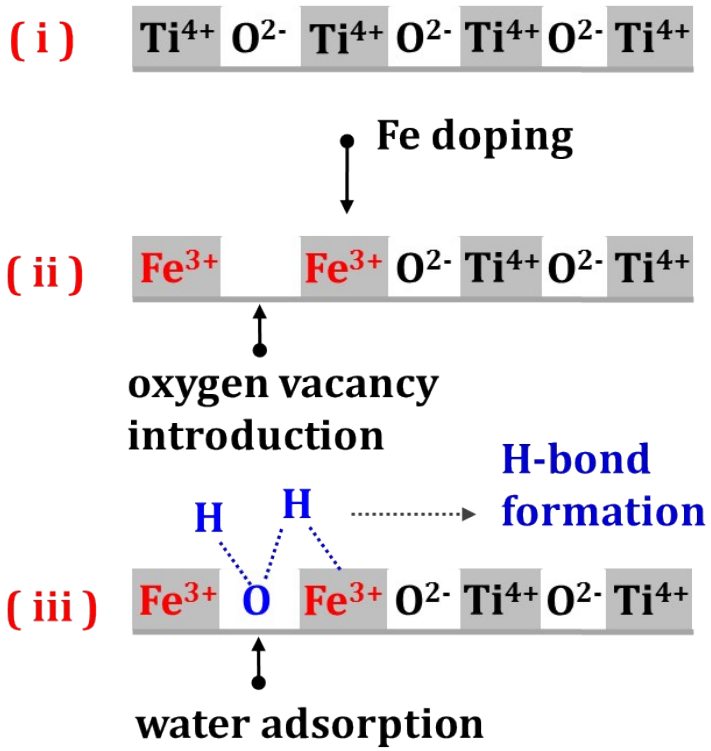

Figure S4 Mode of Fe doping into rutile TiO_2 lattice and the formation of oxygen vacancy for water adsorption

Owing to the difference in the valence electrons of iron and titanium elements, one Fe^{3+} replacing one Ti^{4+} will, theoretically, create one oxygen vacancy in rutile TiO_2 (ii). The oxygen vacancy is the preferred water adsorption site. With one water molecule insert into the oxygen vacancy site, the neighboring Fe^{3+} will act as the electron scavenger and adsorb the hydrogen of the adsorbed water with the formation of the H-bond (iii).

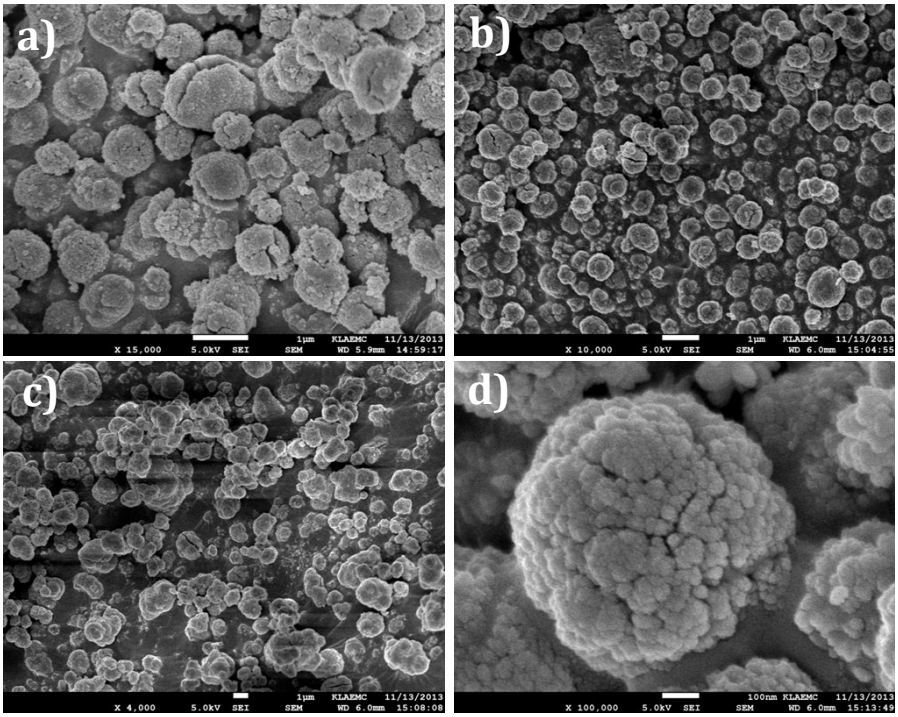

Figure S5 (a, b, c) SEM images of 0.1%Fe-TiO_2, 0.3%Fe-TiO_2 and 0.5%Fe-TiO_2; (d) Enlarged view of 0.3%Fe-TiO_2 sample

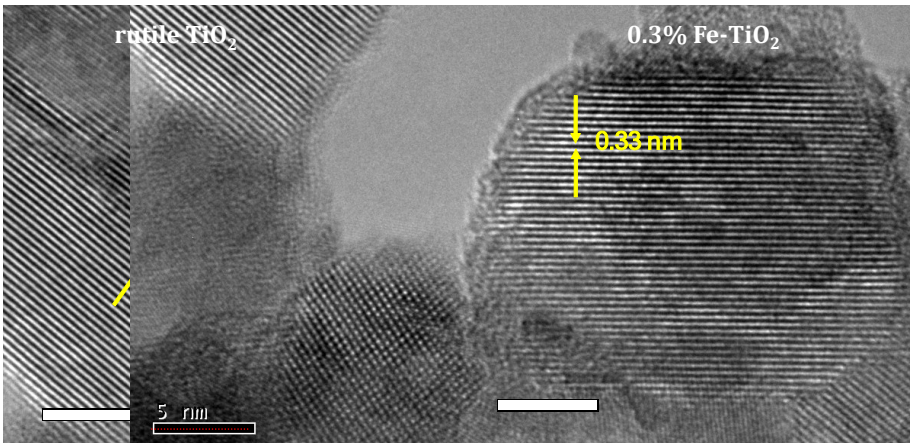

Figure S6 HRTEM images of rutile TiO_2 and 0.3%Fe-TiO_2

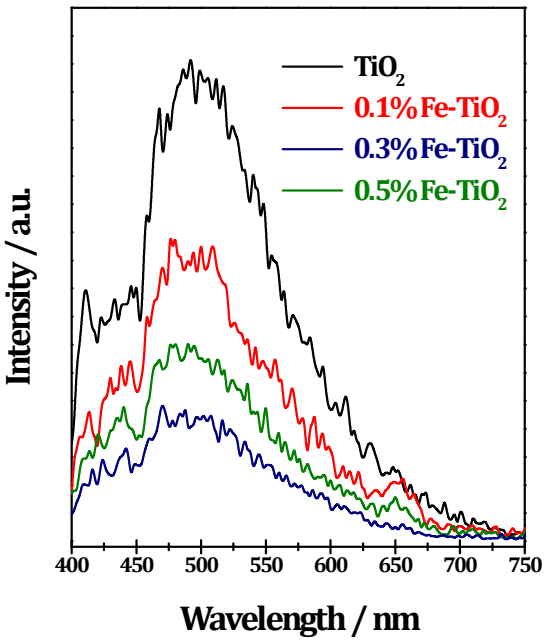

Figure S7 Photoluminescence spectra of rutile TiO_2 and Fe doped rutile TiO_2

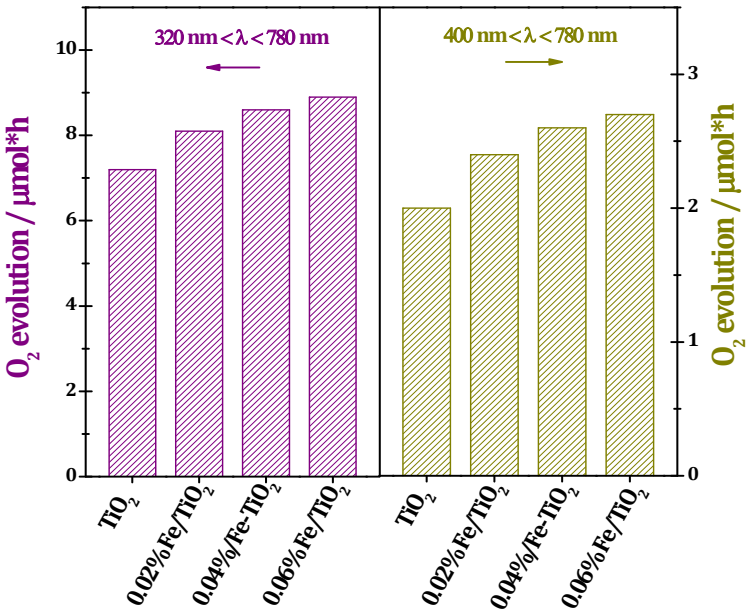

Figure S8 Photocatalytic oxygen evolution from water splitting over rutile TiO_2 and iron surface modified TiO_2 samples under the irradiation of UV-vis or visible light Reaction conditions: 0.1g photocatalyst, 100 mL 0.01M $AgNO_3$ aqueous solution

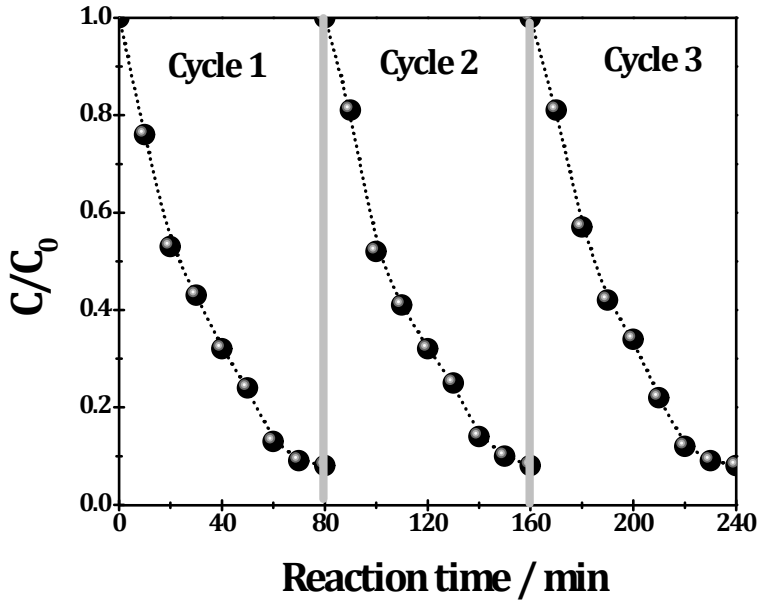

Figure S9 Recycling experiments of RhB degradation over 0.3%Fe-TiO_2 under visible light.

Reaction conditions: 0.05g 0.3%Fe-TiO_2 in 100 mL of 8 mg/L RhB aqueous solution; λ= 400-780 nm